Simulation of Laser Plasma Dynamics: Influence of Ambient Pressure and Intensity of Laser Radiation

V. MAZHUKIN

Institute of Mathematical Modeling, Russian Academy of Sciences, Miusskaya square, 4, 125047 Moscow, Russia

I. SMUROV

Ecole Nationale d'Ingenieurs de Saint-Etienne, 58 rue Jean Parot, 42023 Saint-Etienne Cédex 2, France

AND

G. FLAMANT

Institut de Science et de Génie des Matériaux et Procédés, C.N.R.S., B.P. 5, 66125 Font-Romeu Cédex, France

A mathematical model, describing the dynamics of laser plasma (gas dynamic stage) in air medium with the pressure variation in the range of 1–100 Bar, is presented. The simulation is based on the transient axially symmetric system of radiative gas dynamic equations. The application on the multi-group diffusion approximation for the simulation of radiation transfer is discussed. The solution of gas dynamic equations is made by the explicit finite-difference FLIC method. For the energy equation solving jointly with the averaged equation of radiation diffusion, the implicit difference scheme is used. The later is realized by the proposed nonlinear iterative procedure. The evolution of laser plasma in the near threshold values (for plasma formation) of radiation intensity $G = 5 \times 10^7$–5×10^8 W/cm^2 ($\lambda = 1.06\,\mu$m) is analyzed. It is shown that the mechanism of the plasma expansion strongly depends on the pressure of the gaseous medium: it varies from the light detonation regime of fast combustion at low pressures; to the slow combustion in the form of the subsonic radiative wave at high pressures. © 1994 Academic Press, Inc.

1. INTRODUCTION

At present, due to rising interest to surface machining of materials by means of concentrated energy flows (laser, plasma, electron beam), attention is focused on the physicochemical processes in the vicinity of the surface under treatment. If energy density flux of laser radiation exceeds some threshold value (that generally depends on a number of factors, but usually is larger than 10^6 W/cm^2), a laser produced plasma appears near the target's surface. Later on the energy absorbed by the target depends on: (a) laser irradiation passed through the plasma cloud; (b) radiative transfer from plasma pattern. Both are unknown and difficult to be determined. The experimental results [1]

and the theoretical investigations [2, 3] have shown that in laser action on a highly reflecting metal surfaces, the energy transfer to the target can be increased (or, generally, optimized), if laser plasma is built up over the surface. From the other hand, laser plasma can be used to create surface layers of ceramics such as nitrides and carbides. That is why the simulation of laser plasma dynamics is important for optimization of laser processing parameters.

The dynamics of the plasma formed over the target surface depends on the wavelength, intensity, duration, spatial, and temporal energy distribution of the laser pulse, as well as on a number of gas medium parameters, the most important of the latter are the gas type and the pressure. The laser plasma propagation in gas medium can be of two qualitatively different types: fast [4] and slow [5] combustion.

Referring to the fast combustion regime are the mechanisms of light detonation [4, 6], supersonic radiation waves [7], breakdown waves [8], as well as their various combinations. The fast combustion regimes are characterized by high temperatures (about 10 eV), high pressure differences (hundreds and thousands bar) and supersonic velocities of plasma patterns propagation. As a rule the shock-type gas ionization caused by gas-dynamic compression forces plays a significant role in these regimes. If this is the case, the region of the shock wave strongly absorbs laser radiation.

In slow combustion regimes the main mechanisms are heat conductivity [5] and subsonic heating by radiation [8, 9], which are characterized by slow subsonic expansion of the heated gas. The plasma patterns propagate at nearly

constant pressure close to the pressure of undisturbed gas. The mathematical description of the slow combustion regimes is more simple as compared, for instance, to the light detonation regime of fast combustion, because the mathematical model should only consider the processes of heat and radiation transfer.

If the solid target is located in the focal plane, the situation becomes considerably more sophisticated due to the rise of the number of new physical processes. The kinetics of the phase transformations inside the target material, the interaction of the evaporation products with the ambient gas atmosphere and the conditions of the laser-induced breakdown formation should be taken into account. As a consequence the plasma behavior in the gas media becomes more complicated, because several mechanisms can, at once, play a significant role in the ionization process. From technological applications point of view, the regime of slow combustion is of the greatest interest. However, experiments show that it is difficult to realize this regime in the presence of the target, due to the substantial influence of gas-dynamic effects.

The present paper is concerned with the evolution of the gas-dynamic stage of the laser plasma development, in particular with the transitional regimes in gas media at variable pressures (1–100 bar), under pulsed laser action with near-threshold intensities $G = 10^7$–10^8 W/cm^2 (at the wavelength $\lambda = 1.06 \ \mu$m).

The above mentioned aim is realized through the development of the proposed algorithm for numerical simulations of radiative gas-dynamics phenomena.

2. THE MATHEMATICAL MODEL AND THE PRINCIPAL ASSUMPTIONS

When the self-radiation of laser plasma is taken into account, the corresponding mathematical models become rather complicated. In general, the radiation emitted from plasma: (a) contains information about its state; (b) can influence the energy balance in the system; (c) can break the thermal equilibrium. The description of the radiation processes depends on the emission–absorption mechanisms, as well as on the medium parameters: the characteristic system size L and free-path length l_ν of a photon with energy $h\nu$ (which is determined by the density of particles ρ and their temperature T). The main mechanisms of radiation are known to be the following: discrete emission–absorption in atoms and ions, radiative electron recombination and photoionization, bremsstrahlung (braking radiation), and photon absorption by an electron in an ion field. The radiation processes can be described in the simplest way in two limiting cases, when the optical thickness of plasma is either small ($l_\nu \gg L$) or large ($l_\nu \ll L$).

The optically thin plasma is characterized by a low density of electrons ($n_e \sim 10^{13}$ cm^{-3}) and relatively large

geometrical dimensions. When the dimension L is not too large ($L < 1$ m), all kinds of radiation easily leave plasma. If it is the case, the reliable description can be obtained on the basis of the coronary model approximation [10]. It is assumed that the probability of the collision transitions between levels is small as compared to the spontaneous transitions, and each act of collision excitation of either atom or ion is balanced out by the corresponding act of radiation decay. The radiation spectrum of such a plasma consists of a set of narrow lines on a background of the continuous spectrum.

The optically thick plasma ($l_\nu \ll L$) is characterized by Saha-Boltzman charge composition. The corresponding spectrum of equilibrium black body radiation contains no lines, as broadening is too large and the lines merge with the continuous spectrum. The radiative losses in this case result only on the plasma energy balance. The mathematical description of the plasma in such a state can be performed, for example, in the framework of the so-called, radiative heat transfer model [11].

If both collision and radiative transitions play substantial role simultaneously, then it corresponds to an intermediate position between these two limiting cases, and therefore it is the most complicated to be described. Usually the approximation of so-called collision-radiative model is applied to analyze the behavior of such plasmas [12, 13]. Various non-equilibrium effects in plasma of an arbitrary transparency can be described by means of this model. When the dimensions of plasma pattern are not too small it becomes necessary to account for the reabsorption of both discrete and continuous spectra. In such a case the equations of collision-radiative model should be completed by the equation of the radiation transfer. The approximation of collision-radiation model is oftenly used to describe over-heated or undercooled plasma of relatively high density $n_e > 10^{18}$ cm^{-3} [14].

Generally the laser plasma that is formed in a flux of evaporated matter or in an ambient gas atmosphere can have quite different optical thickness, due to sharp variations of the density ρ and temperature T with time and space caused by considerable gas-dynamic processes. When the dimensions of plasma pattern are large enough, the reabsorption of both discrete spectrum and continuous spectrum becomes significant. The further point of complications is the fact that the laser radiation is absorbed by the electron component with the temperature T_e which turns out to be higher than the temperature of atoms and ions T_g. In general the relaxation process due to elastic electron atom and electron ion collisions can be rather prolonged, so the plasma cloud side facing the incident radiation is in thermal non-equilibrium state. The description of the radiation and of the evolution of plasma pattern, as well as the subsequent problem solution, appears to be the most complicated in this case, because the medium

macro parameters (gas-dynamic and temperature fields) are related to the micro processes in a sophisticated way. From the mathematical point of view it means that the processes of gas-dynamics should be analyzed simultaneously with the processes of the kinetics of radiation-collision transitions and radiative transfer.

Thus the evolution of the laser plasma represents an extremely sophisticated phenomenon, and to investigate it efficiently by means of numerical simulations one should make reasonable assumptions and simplifications for the definition of the problem. The main of them are the following:

1. For relatively large dimensions $l_v \leqslant L$ and high plasma density the conditions of local thermodynamic equilibrium should be respected at least close to the surface, the dominating process being the reabsorption of the continuous spectrum.

2. Taking into account the radiation transfer in the problems of gas-dynamics makes the algorithm of the solution much more complicated. The difficulties are associated with the equation of radiative transfer, which is primarily multi-dimensional:

$$\frac{1}{c}\frac{\partial I_v}{\partial t} + \Omega \text{ grad } I_v + \kappa_v I_v = \kappa_v I_{v\text{eq}},$$

$$\kappa_v = \kappa_v(v, T, \rho), \qquad I_v = I_v(t, \mathbf{r}, v, \Omega), \tag{1}$$

where c denotes the light velocity, I_v is the spectral intensity of the radiation,

$$I_{v\text{eq}} = \frac{2h}{c^2} \cdot \frac{v^3}{(e^{hv/kT} - 1)} \tag{2}$$

is the spectral intensity of equilibrium radiation, h is Planck's constant, k is Boltzmann's constant, $\mathbf{r}$ is the radius-vector, Ω is the vector of unit length in the direction of photon motion, κ_v is the absorption coefficient for a photon with frequency v, T and ρ are the temperature and density of the matter, and t is time.

The difficulties arising in the numerical solution of the radiative gas-dynamics problems is a stimulation to use various approximations. In particular, assuming that the field of the laser plasma radiation has low anisotropy, one can utilize the model of diffusion approximation for the description of the radiation transfer (isotropic distribution of radiation) [11],

$$\frac{\partial U_v}{\partial t} + \text{div } \mathbf{W}_v + c\kappa_v U_v = c\kappa U_{v\text{eq}},$$

$$\frac{1}{c}\frac{\partial \mathbf{W}_v}{\partial t} + \frac{c}{3}\text{ grad } U_v + \kappa_v \mathbf{W}_v = 0, \tag{3}$$

where U_v is the spectral density of the radiation,

$$U_{v\text{eq}} = \frac{8\pi h\, v^3}{c^3(e^{hv/kT} - 1)}$$

is the spectral density of equilibrium radiation, $\mathbf{W}$ is the vector of the radiation energy flux.

The index v will be raised up in further notation, after the appearance of spatial (r, z) and grid (i, n) indexes.

The equations of the diffusion model are of smaller dimensionality than the initial transfer equation, as it does not depend on the angular coordinates Ω.

3. Taking into account that characteristic time of the medium parameters variation is larger than the time of the radiation pass through the region under study, the radiation transfer can be described as a quasi-stationary phenomenon.

4. In addiation, the density of energy and the radiation pressure are small in comparison with the density of energy and the pressure of the medium. Moreover, in the temperature and plasma density ranges under study, radiation scattering is considered to be insignificant.

Consider a two-dimensional transient problem of the laser radiation interaction with the air plasma. The incident laser flux with the wavelength $\lambda = 1.06\ \mu$m is assumed to be symmetric with respect to z-axis (which is directed along the beam propagation), the intensity being distributed according to a Gaussian law $G = G_0 \cdot \exp(-r^2/R^2)$, where R is the radius of the focal spot. The peculiarities of the interaction, as well as the laser plasma behavior in a dense air atmosphere with the pressure varying over a wide range, are studied from the moment when a thin $(z_0 = 10\text{–}50\ \mu\text{m})$ absorbing plasma layer is formed close to the target.

The mathematical formulation of the problem is as follows. Accounting for the approximations made, the interaction of the laser radiation with the gas medium is described by the system of equations for radiative gas dynamics (RGD) which are symmetric with respect to z-axis [15, 16]:

$$\frac{\partial \rho}{\partial t} + \frac{1}{r}\frac{\partial}{\partial r}(r\rho u) + \frac{\partial}{\partial z}(\rho v) = 0 \tag{4}$$

$$\frac{\partial \rho u}{\partial t} + \frac{1}{r}\frac{\partial}{\partial r}(r\rho u^2) + \frac{\partial}{\partial z}(\rho uv) = -\frac{\partial(p + \omega)}{\partial r} \tag{5}$$

$$\frac{\partial \rho v}{\partial t} + \frac{1}{r}\frac{\partial}{\partial r}(r\rho uv) + \frac{\partial}{\partial z}(\rho v^2) = -\frac{\partial(p + \omega)}{\partial z} \tag{6}$$

$$\frac{\partial \rho \varepsilon}{\partial t} + \frac{1}{r}\frac{\partial}{\partial r}(r\rho u\varepsilon) + \frac{\partial}{\partial z}(\rho v\varepsilon)$$

$$= -p\left[\frac{1}{r}\frac{\partial ru}{\partial r} + \frac{\partial v}{\partial z}\right] - \frac{1}{r}\frac{\partial W_r}{\partial r} - \frac{\partial W_z}{\partial z} - \frac{\partial G}{\partial z} \tag{7}$$

$$\frac{1}{r}\frac{\partial(rW_r^v)}{\partial r}+\frac{\partial W_z^v}{\partial z}+c\kappa_v U_v=c\kappa_v U_{v\mathrm{eq}} \tag{8}$$

$$\frac{1}{3}\frac{c}{\kappa_v}\frac{\partial U_v}{\partial r}=-W_r^v, \qquad \frac{1}{3}\frac{c}{\kappa_v}\frac{\partial U_v}{\partial z}=-W_z^v, \tag{9}$$

$$\mathbf{W}=\int_0^\infty \mathbf{W}_v\,dv$$

$$\frac{\partial G}{\partial z}+\kappa G=0 \qquad (r,z)\in\Omega,\ \Omega=[0,L_r]\times[0,L_z]. \tag{10}$$

The notations involved: t = time; r, z = spatial coordinates; index v refers to spectral values, u, v = components of the velocity vector, ε = internal energy, p = pressure, ω = artificial viscosity, G = laser radiation intensity.

The boundary and initial conditions for the equations (4)–(10) have the form

$$\begin{aligned}
t=0,\quad & T=T_p, && 0\leqslant(r\times z)\leqslant(R\times z_0)\\
& T=T_0, && (R\times z_0)\leqslant(r\times z)\leqslant(L_r\times L_z) \quad (11)\\
& P=P_0, && 0\leqslant(r\times z)\leqslant(L_r\times L_z)
\end{aligned}$$

$$\begin{aligned}
t>0,\quad & r=0, && v=0,\quad W_r=0\\
& z=0, && u=0,\quad cU=\sigma T^4\\
& r=L_r, && p=p_0,\quad W_r=-cU/2 \quad (12)\\
& z=L_z, && p=p_0,\quad W_z=-cU/2,\\
& && G=G_0\exp(-(r/R)^2).
\end{aligned}$$

3. THE SOLUTION ALGORITHM

When developing the solution algorithm we used to a large extent the approach presented in [16, 17] for the problems of the dynamics of emitting gas. The overall computation scheme to solve the system of RGD equations at each time step $t=t^j$ can be presented as a combination of several stages.

In the first stage the equations of multi-group diffusion are averaged on a difference level with respect to photon energies, based on the gas-dynamic values and the temperature as obtained from the previous t^{j-1} layer. Averaging is produced by means of the solution of N_k elliptic-type equations. For the reduction of the computation time, the coefficients of the thus-obtained averaged equation were considered "frozen" during J time step. Therefore the averaging procedure was executed once in every J time steps rather than in every step.

In the second stage the diffusion equation and the equation for energy transfer are solved together. In the third stage the gas-dynamics equations are solved.

Let us consider each of these stages in detail:

1. As compared to the equations of gas-dynamics (4)–(6), the equations of radiation diffusion (8), (9) contain one variable more, namely v, this extra variable causes a lot of complications in solving the task as a whole. To overcome this difficulty we use the multi-group approximation [9, 15]. According to it, the whole spectrum is split into a finite number N_k of frequency ranges (groups). For the frequencies belonging to the same group $v_k<v<v_{k+1}$ the absorption coefficient $\kappa_v(T,\rho,v)$ is assumed to be independent on frequency:

$$\kappa_v(T,\rho,v)=\kappa_v(T,\rho), \qquad k=1,2,...,N_k,$$

and its magnitude is determined by means of the frequency averaging procedure, using Planck approximation:

$$\kappa_k(T,\rho)=\int_{v_k}^{v_{k+1}}\kappa_v U_{v\mathrm{eq}}\,dv\Big/\int_{v_k}^{v_{k+1}}U_{v\mathrm{eq}}\,dv.$$

In this case the radiation transfer is determined by the system of equations for the multi-group diffusion approximation,

$$\frac{1}{r}\frac{\partial(rW_r^k)}{\partial r}+\frac{\partial W_z^k}{\partial z}+c\kappa_k U_k=c\kappa_k U_{k\mathrm{eq}} \tag{13}$$

$$\frac{1}{3}\frac{c}{\kappa_k}\frac{\partial U_k}{\partial r}=-W_r^k, \qquad \frac{1}{3}\frac{c}{\kappa_k}\frac{\partial U_k}{\partial z}=-W_z^k, \tag{14}$$

which can be easily reduced to equations of elliptic type,

$$-\mathrm{div}\left(\frac{1}{3}\frac{c}{\kappa_k}\right)\mathrm{grad}\,U_k+c\kappa_k U_k=\kappa_k U_{k\mathrm{eq}},$$

where

$$U_{k\mathrm{eq}}=\int_{v_k}^{v_{k+1}}U_{v\mathrm{eq}}\,dv=\frac{8\pi h}{c^3}\int_{v_k}^{v_{k+1}}\frac{v^3}{\exp(hv/kT)-1}\,dv.$$

Taking into account, that

$$\frac{8\pi h}{c^3}\int_{v_k}^{v_{k+1}}\frac{v^3}{\exp(hv/kT)-1}\,dv=\frac{8\pi k^4 T^4}{c^3 h^3}\int_{x_k}^{x_{k+1}}\frac{x'^3}{\exp(x')-1}\,dx'$$

$$=\frac{4\sigma(T,hv_k,hv_{k+1})\cdot T^4}{c},$$

the considered elliptic equations can be written in the form

$$-\mathrm{div}\left(\frac{1}{3}\frac{c}{\kappa_k}\right)\mathrm{grad}\,U_k+c\kappa_k U_k=4\kappa_k\sigma(T,hv_k,hv_{k+1})\cdot T^4, \tag{15}$$

where

$$\sigma(T, h\nu_k, h\nu_{k+1}) = \sigma_k = \frac{2\pi k^4}{c^2 h^3} \int_{x_k}^{x_{k-1}} \frac{x'^3}{\exp(x')-1} dx' = \frac{2\pi k^4}{c^2 h^3}$$

$$\times [\sigma(h\nu_{k+1}/kT) - \sigma(h\nu_{k+1}/kT)].$$

To determine the $\sigma(x)$ function, the integral expression

$$\sigma(x) = \int_0^x \frac{x'^3}{\exp(x')-1} dx'$$

was approximated by the relations [16]

$$\sigma(x) = \begin{cases} 1.3799x^3(1/3 - x/8 + x^2/62.4), & x \leqslant 2 \\ 1.3799[6.4939 - e^{-x}(x^3 + 3x^3 + 6x + 7.28), & x > 2 \end{cases}$$

The solution of the system of elliptic equations (15) is a time-consuming computational procedure, so it is quite a natural wish to reduce the body of computations that are required to solve the multi-group equations; moreover, only the overall flux $\mathbf{W} = \sum_{k=1}^{N_k} \mathbf{W}_k$ and the overall density of energy $U = \sum_{k=1}^{N_k} U_k$ are required to be known in the initial problem. For the continuous spectrum the method of frozen coefficients is an efficient way of averaging [18].

Consider finite-difference approximation of Eq. (15) on the five-point stencil,

$$B_{in}^k U_{i,n-1}^k + K_{in}^k U_{i-1,n}^k - C_{in}^k U_{i,n}^k + E_{in}^k U_{i+1,n}^k$$
$$+ Z_{in}^k U_{i,n+1}^k + F_{in}^k = 0, \qquad (16)$$

where the coefficients B_{in}^k, K_{in}^k, Z_{in}^k are defined as usual, i.e.,

$$B_{in}^k = 2c\{3(z_{n+1} - z_n)[x_{i,n}^k(z_{n-1} - z_n)$$
$$+ \kappa_{i,n-1}(z_n - z_{n-1})]\}^{-1},$$

$$K_{in}^k = 4r_i/\{[3\kappa_{in}^k(r_{i-1} - r_i) + \kappa_{i-1,n}^k(r_i - r_{i-1})](r_{i+1} - r_i)$$
$$- (r_{i+1} + r_i)\}, \qquad i, n \text{ is the cell number.}$$

To solve Eqs. (16) the non-linear iteration method [19] was applied; it was used for a nine-point finite-difference stencil [17]. The essence of the method as applied to the five-point scheme can be presented concerning a single group, say, $k = 1$. It is assumed that the solution of the system (16) satisfies simultaneously the conditions

$$U_{i,n} = \alpha_{i+1,n} U_{i+1,n} + \beta_{i+1,n},$$
$$U_{i,n} = \gamma_{i-1,n} U_{i-1,n} + d_{i-1,n}, \qquad (17)$$
$$U_{i,n} = \alpha_{i,n+1}^* U_{i,n+1} + \beta_{i,n+1}^*,$$
$$U_{i,n} = \gamma_{i,n-1}^* U_{i,n-1} + d_{i,n-1}^*. \qquad (18)$$

Substituting the relations (17), (18) in Eq. (16) one obtains the system of three-point equations. To solve it the short Gaussian method for three-diagonal matrixes can be applied:

$$\gamma_{i-1,n}^{(s+1/2)} = K_{in}(C_{in} - \alpha_{in}^{*(s)} B_{in} - \gamma_{in}^{*(s+1/2)} Z_{in}$$
$$- \gamma_{in}^{(s+1/2)} E_{in})^{-1},$$

$$\gamma_{M-1,n}^{(s+1/2)} = \gamma_n$$

$$\alpha_{i+1,n}^{(s+1/2)} = E_{in}(C_{in} - \alpha_{in}^{*(s)} B_{in} - \gamma_{in}^{*(s+1/2)} Z_{in}$$
$$- \alpha_{in}^{(s+1/2)} K_{in})^{-1},$$

$$\alpha_{1n}^{(s+1/2)} = 1,$$

$$\gamma_{i,n-1}^{*(s+1/2)} = B_{in}(C_{in} - \alpha_{in}^{(s+1/2)} K_{in} - \gamma_{in}^{(s+1/2)} E_{in}$$
$$- \gamma_{in}^{*(s+1/2)} Z_{in})^{-1},$$

$$\gamma_{i,N-1}^{*(s+1/2)} = 1,$$

$$\gamma_{i-1,n}^{(s+1)} = K_{in}(C_{in} - \alpha_{in}^{*(s+1)} B_{in} - \gamma_{in}^{*(s+1/2)} Z_{in}$$
$$- \gamma_{in}^{(s+1)} E_{in})^{-1},$$

$$\gamma_{M-1,n}^{(s+1)} = \gamma_n,$$

$$\alpha_{i+1,n}^{(s+1)} = E_{in}(C_{in} - \alpha_{in}^{*(s+1)} B_{in} - \gamma_{in}^{*(s+1/2)} Z_{in}$$
$$- \alpha_{in}^{(s+1)} K_{in})^{-1},$$

$$\alpha_{1n}^{(s+1)} = 1,$$

$$\alpha_{i+1,n}^{*(s+1)} = Z_{in}(C_{in} - \alpha_{in}^{(s+1)} K_{in} - \gamma_{in}^{(s+1)} E_{in}$$
$$- \alpha_{in}^{*(s+1)} B_{in})^{-1},$$

$$\alpha_{i1}^{*(s+1)} = 1,$$

where s is the iteration number, $s + \frac{1}{2}$ is the number of intermediate iterations.

After the α-process is accomplished, the iteration process is developed to obtain β, d, β^*, d^*, based on already known values of α, γ, α^*, γ^*,

$$d_{i-1,n}^{(s+1/2)} = \frac{d_{in}^{(s+1/2)} E_{in} + d_{in}^{*(s+1/2)} X_{in}^{(s)} + Y_{in}^{(s)}}{C_{in} - \alpha_{in}^* B_{in} - \gamma_{in}^* Z_{in} - \gamma_{in} E_{in}},$$

$$d_{M-1,n}^{(s+1/2)} = 0,$$

$$\beta_{i+1,n}^{(s+1/2)} = \frac{\beta_{in}^{(s+1/2)} K_{in} + d_{in}^{*(s+1/2)} X_{in}^{(s)} + Y_{in}^{(s)}}{C_{in} - \alpha_{in}^* B_{in} - \gamma_{in}^* Z_{in} - \alpha_{in} K_{in}},$$

$$\beta_{1,n}^{(s+1/2)} = 0,$$

$$d_{i,n-1}^{*(s+1/2)} = \frac{d_{in}^{*(s+1/2)} Z_{in} + \beta_{in}^{(s+1/2)} K_{in} + d_{in}^{(s+1/2)} E_{in} + F_{in}}{C_{in} - \alpha_{in} K_{in} - \gamma_{in} Z_{in} - \gamma_{in}^* E_{in}},$$

$$d_{i,N-1}^{*(s+1/2)} = 0,$$

$$d_{i-1,n}^{(s+1)} = \frac{d_{in}^{(s+1)}E_{in} + \beta_{in}^{*(s+1)}X_{in}^{(s+1/2)} + Y_{in}^{(s+1/2)}}{C_{in} - \alpha_{in}^*B_{in} - \gamma_{in}^*Z_{in} - \gamma_{in}E_{in}},$$

$$d_{M-1,n}^{(s+1)} = 0,$$

$$\beta_{i+1,n}^{(s+1)} = \frac{\beta_{in}^{(s+1)}K_{in} + \beta_{in}^{*(s+1)}X_{in}^{(s+1/2)} + Y_{in}^{(s+1/2)}}{C_{in} - \alpha_{in}^*B_{in} - \gamma_{in}^*Z_{in} - \alpha_{in}K_{in}},$$

$$\beta_{i,n+1}^{*(s+1)} = \frac{\beta_{in}^{*(s+1)}B_{in} + \beta_{in}^{(s+1)}K_{in} + d_{in}^{(s+1)}E_{in} + F_{in}}{C_{in} - \alpha_{in}K_{in} - \alpha_{in}^*B_{in} - \gamma_{in}E_{in}},$$

where

$$X_{in}^{(s)} = Z_{in} + f_{in}^{-1(s)}\omega B_{in},$$

ω is the grid parameter, $0 \leqslant \omega \leqslant 1$, $\omega = 0$ for $n = N - 1$;

$$Y_{in}^{(s)} = (1 - \omega)X_{in}\beta_{in}^{*(s)} + F_{in},$$

$$f_{in}^{(0)} = (1 - \gamma_{in}^*)/(1 - \alpha_{in}^*),$$

$$X_{in}^{(s+1/2)} = B_{in} + f_{in}^*\omega Z_{in},$$

$$Y_{in}^{(s+1/2)} = (1 - \omega)Z_{in}d_{in}^{*(s+1/2)} + F_{in}.$$

The function f_{in} is introduced to improve the convergence. It is recalculated for the next iteration of the β-process:

$$f_{in} = \frac{U_{i,n+1}^{(s+1)} - \gamma_{in}^*U_{in}^{(s+1)}}{U_{i,n+1}^{(s+1)} - \alpha_{in}^*U_{in}^{(s+1)}}.$$

Using the above formulas, averaging of the multi-group system (16) with respect to k is performed:

$$B_{in}U_{i,n-1} + K_{in}U_{i-1,n} - C_{in}U_{i,n} + E_{in}U_{i+1,n}$$
$$+ Z_{in}U_{i,n+1} - \kappa_{in}U_{i,n} + F_{in} = 0. \tag{19}$$

The coefficients of this equation are defined as

$$B_{in} = \left(\sum_{k=1}^{N_k} U_{i,n-1}\right)^{-1}\sum_{k=1}^{N_k} U_{i,n-1}B_{in}^k,$$

$$K_{in} = \left(\sum_{k=1}^{N_k} U_{i-1,n}\right)^{-1}\sum_{k=1}^{N_k} U_{i-1,n}K_{in}^k,$$

$$\vdots \tag{20}$$

$$Z_{in} = \left(\sum_{k=1}^{N_k} U_{i,n+1}\right)^{-1}\sum_{k=1}^{N_k} U_{i,n+1}Z_{in}^k,$$

$$F_{in} = \sum_{k=1}^{N_k} F_{in}^k.$$

The averaging of the multi-group equations is not performed in each time step. In order to reduce the volume of computation the averaged coefficients $B_{in}, ..., Z_{in}$ are assumed to be unchanged during J time steps. In J steps the system of multi-group equations is again solved numerically and new averaged coefficients are determined.

2. When solving RGD problems, the temperature is determined by means of joint solution of the equations for energy transfer and radiation diffusion. The gas-dynamic properties, namely the density ρ, velocity v, and the work of compression forces are assumed to be known. The simultaneous solution of these equations is required because the radiation energy flux $\mathbf{W}$ depends on temperature and pressure in each point of the region under study, so $\mathbf{W}$ cannot be presented by simple relations. Therefore the most straightforward way to solve the equation for energy is an explicit scheme, where the flux $\mathbf{W}$ is determined from the data of the preceding time step. However, as shown by numerous calculations, in this case the stability conditions require rigid limitations on the step of integration over t.

It is well known that an implicit method is more efficient to solve the problem when the equations for both energy and radiation diffusion are solved simultaneously. The equation for energy and the averaged equation for radiation diffusion are

$$\frac{\partial \varepsilon}{\partial t} = -\frac{1}{\rho}(\text{div } W + Q),$$

$$-\text{div }\frac{c}{3\kappa}\text{grad } U + c\kappa U = 4\kappa\sigma T^4,$$

where Q is the contribution of all the sources but radiation to the equation for energy, U is the radiation density. In the finite-difference form the system of equations to determine the radiation flux and the internal energy is written as

$$\frac{\varepsilon_{in}^{(s+1)} - \varepsilon_{in}^{j-1}}{\tau^{j-1}}$$
$$= \frac{1}{\rho_{in}}[B_{in}U_{i,n-1}^{(s+1)} + K_{in}U_{i-1,n}^{(s+1)} - C_{in}U_{i,n}^{(s+1)}$$
$$+ E_{in}U_{i+1,n}^{(s+1)} + Z_{in}U_{i,n+1}^{(s+1)} + Q_{in}^{j-1}] \tag{21}$$

$$B_{in}U_{i,n-1}^{(s+1)} + K_{in}U_{i-1,n}^{(s+1)} - C_{in}U_{i,n}^{(s+1)} + E_{in}U_{i+1,n}^{(s+1)}$$
$$+ Z_{in}U_{i,n+1}^{(s+1)} - \kappa_{in}U_{i,n}^{(s+1)} + F_{in}^{(s+1)} = 0.$$

It is necessary to remind that $B_{in}, ..., Z_{in}$ are calculated only once every J steps according to formulas (20). The function F_{in} is calculated for every time step,

$$F_{in} = \sum_{k=1}^{N_k} \kappa_k(T_{in}, \rho_{in})\sigma_k(T_{in}, h\nu_k, h\nu_{k+1})T_{in}^4.$$

In Eq. (22) the value of F_{in} is unknown. By linearization F_{in} and ε_{in} with respect to T, one obtains

$$F_{in}^{(s+1)} = F_{in}^{(s)} + \left(\frac{\partial F}{\partial T}\right)_{in}^{(s)} \left(T_{in}^{(s+1)} - T_{in}^{(s)}\right) \qquad (23)$$

$$\varepsilon_{in}^{(s+1)} = \varepsilon_{in}^{(s)} + \left(\frac{\partial \varepsilon}{\partial T}\right)_{in}^{(s)} \left(T_{in}^{(s+1)} - T_{in}^{(s)}\right). \qquad (24)$$

Based on expressions (21), (24) and (22), (23), the implicit scheme of the solution of equations for energy and diffusion of radiation is written as

$$T_{in}^{(s+1)} = T_{in}^{(s)} + \left[\rho \left(\frac{\partial F}{\partial T}\right)^{(s)}\right]_{in} \left[\varepsilon_{in}^{j-1} - \varepsilon_{in}^{(s)}\right.$$
$$+ \tau^{j-1}(B_{in} U_{i,n-1}^{(s+1)} + K_{in} U_{i-1,n}^{(s+1)} - C_{in} U_{i,n}^{(s+1)}$$
$$+ E_{in} U_{i+1,n}^{(s+1)} + Z_{in} U_{i,n+1}^{(s+1)} + Q_{in}^{j-1})], \qquad (25)$$

$$(1 + g_{in}^{(s)})[B_{in} U_{i,n-1}^{(s+1)} + K_{in} U_{i-1,n}^{(s+1)} - C_{in} U_{i,n}^{(s+1)}$$
$$+ E_{in} U_{i+1,n}^{(s+1)} + Z_{in} U_{i,n+1}^{(s+1)}] - \kappa_{in} U_{i,n}^{(s+1)} + F_{in}^{(s+1)}$$
$$+ g_{in}^{(s)} \left[Q_{in}^{j-1} - \frac{\varepsilon_{in}^{(s)} - \varepsilon_{in}^{j-1}}{\tau^{j-1}}\right] = 0, \qquad (26)$$

where

$$g_{in}^{(s)} = \left(\frac{\partial F}{\partial T}\right)_{in}^{(s)} \tau^{j-1} \bigg/ \left(\frac{\partial \varepsilon}{\partial T} \rho\right)_{in}^{(s)}.$$

The density of the radiation energy U and the temperature are determined from the joint solution of the system (25), (26).

3. In the RGD problems the radiation field is closely connected to the gas-dynamic properties of the medium. For finite-difference approximation of the gas-dynamic equations (written in Euler variables) four-angular orthogonal grids are often used. Thus-obtained finite-difference schemes have the simplest form. In the present paper the FLIC method [20, 21] was used for the solution of equations for gas-dynamics. The characteristic feature of this method is the Euler–Lagrange approach.

In the first Lagrange stage the convective flows of mass, momentum, and energy are not taken into account and the system

$$\frac{\partial \rho}{\partial t} = 0,$$

$$\rho \frac{\partial u}{\partial t} = -\frac{\partial(P + \omega)}{\partial r}, \qquad \rho \frac{\partial v}{\partial t} = -\frac{\partial(P + \omega)}{\partial z},$$

$$\rho \frac{\partial \varepsilon}{\partial t} = -(P + \omega) \left(\frac{1}{r}\frac{\partial(ru)}{\partial r} + \frac{\partial v}{\partial z}\right) - \frac{\partial G}{\partial z},$$

is considered which is approximated by the expressions

$$u_{in}^{j-1/2} = u_{in}^{j-1} - \frac{\tau^{j-1}}{\rho_{in}^{j-1}(r_{i+1} - r_i)} \left\{\frac{1}{2}\left[\frac{r_{i+1}}{r_{i+1/2}}\left(P_{i+1n}^{j-1} - P_{in}^{j-1}\right)\right.\right.$$
$$\left.\left. + \frac{r_i}{r_{i+1/2}}(P_{in}^{j-1} - P_{i-1n}^{j-1})\right] + (\omega_{i+1n}^{j-1} - \omega_{in}^{j-1})\right\}$$

$$v_{in}^{j-1/2} = v_{in}^{j-1} - \frac{\tau^{j-1}}{\rho_{in}^{j-1}(z_{n+1} - z_n)}$$
$$\times \left\{\frac{(P_{in+1}^{j-1} - P_{in}^{j-1})}{2} + \omega_{i+1n}^{*j-1} - \omega_{in}^{*j-1}\right\}$$

$$\varepsilon_{in}^{j-1/2} = \varepsilon_{in}^{j-1} - \frac{\tau^{j-1}}{\rho_{in}^{j-1}} \left\{\frac{1}{2}\frac{1}{z_{n+1} - z_n}\left[P_{in}^{j-1}(v_{in+1} - v_{in-1})\right.\right.$$
$$\left. + \omega_{i,n+1}^{*j-1}(v_{in+1} - v_{in}) + \omega_{in}^{*j-1}(v_{in} - v_{in-1})\right]$$
$$+ \frac{1}{2}\frac{1}{r_{i+1} - r_i}\left[P_{in}^{j-1}\left(\frac{r_{i+1}}{r_{i+1/2}}(u_{i+1n} - u_{in})\right.\right.$$
$$\left. - \frac{r_i}{r_{i+1/2}}(u_{in} - u_{i-1n})\right)$$
$$+ \omega_{i+1n}\left(\frac{r_{i+3/2}}{r_{i+1/2}}u_{i+1n} - u_{in}\right)$$
$$\left.\left. + \omega_{in}\left(u_{in} - \frac{r_{i-1/2}}{r_{i+1/2}}u_{i-1n}\right)\right]$$
$$- \frac{1}{z_{n+1} - z_n}(G_{n+1}^{J-1} - G_n^{J-1})\right\}.$$

Here $u^{j-1/2}$, $v^{j-1/2}$, $\varepsilon^{j-1/2}$ are the intermediate values of velocities and energy: $r_{i+1/2} = 0.5(r_i + r_{i+1})$, $u_{in} = 0.5(u_{in}^{j-1} + u_{in}^{j-1/2})$, $v_{in} = 0.5(v_{in}^{j-1} + v_{in}^{j-1/2})$.

The artificial viscosity ω is defined as

$$\omega_{in}^{j-1} = a u_{c,in}^{j-1} \frac{(\rho_{i-1,n} - \rho_{in})^{j-1}}{2}(u_{i-1,n}^{j-1} - u_{in}^{j-1})$$

if the following inequalities hold simultaneously:

$$k[(u_{i-1,n} + u_{in})^2/4 + (v_{i-1,n} - v_{in})^2/4]^{j-1} < (u_{c,in}^{j-1})^2,$$
$$u_{i-1,n}^{j-1} > u_{in}^{j-1}.$$

Otherwise $\omega_{in}^{j-1} = 0$.

Here u_c is the sound velocity; a, k are constants. The coefficient a characterizes the scale of smoothing of the shock wave front, $0 < k < 2a$; ω_{in}^{*j-1} is calculated in an analogous way.

In the second Euler stage, the flows of matter, momentum, and energy drawn through the cell walls are taken into account and their final magnitudes are found. Thus, these

flows crossing the cell wall in the direction $r \leqslant r \leqslant r_{i-1}$, $z_n \leqslant z \leqslant z_{n+1}$ are equal:

$$\Delta M_{in}^{(r)} = \tau^{j-1} \frac{(u_{i-1n}^{j-1/2} + u_{in}^{j-1/2})}{2} \begin{cases} \rho_{i-1n}^{j-1}, & u_{i-1n}^{j-1/2} + u_{in}^{j-1/2} > 0, \\ \rho_{in}^{j-1}, & u_{i-1n}^{j-1/2} + u_{in}^{j-1/2} \leqslant 0, \end{cases}$$

$$\Delta V_{in}^{(r)} = \tau^{j-1} \frac{(u_{i-1n}^{j-1/2} + u_{in}^{j-1/2})}{2}$$

$$\begin{cases} \rho_{i-1n}^{j-1} u_{i-1n}^{j-1/2}, & u_{i-1n}^{j-1/2} + u_{in}^{j-1/2} > 0, \\ \rho_{in}^{j-1} u_{in}^{j-1/2}, & u_{i-1n}^{j-1/2} + u_{in}^{j-1/2} \leqslant 0, \end{cases}$$

$$\Delta E_{in}^{(r)} = \tau^{j-1} \frac{(u_{i-1n}^{j-1/2} + u_{in}^{j-1/2})}{2}$$

$$\begin{cases} \rho_{i-1n}^{j-1} E_{i-1n}^{j-1/2}, & u_{i-1n}^{j-1/2} + u_{in}^{j-1/2} > 0, \\ \rho_{in}^{j-1} E_{in}^{j-1/2}, & u_{i-1n}^{j-1/2} + u_{in}^{j-1/2} \leqslant 0, \end{cases}$$

where $E_{in}^{j-1/2} = \varepsilon_{in}^{j-1/2} + ((u_{in}^{j-1/2})^2 + (v_{in}^{j-1/2})^2)/2$.

The flows of mass and energy in the z-direction are found analogously. After that the gas-dynamic values ρ, u, v, E, ε are recalculated:

$$\rho_{in}^j \rho_{in}^{j-1} - \frac{1}{z_{n+1} - z_n} (\Delta M_{i,n+1}^{(z)} - \Delta M_{i,n}^{(z)})$$

$$- \frac{2(r_{i+1} \Delta M_{i+1,n}^{(r)} - r_i \Delta M_{in}^{(r)})}{(r_{i+1} - r_i)(r_{i+1} + r_i)}$$

$$\vdots$$

$$E_{in}^j = \frac{1}{\rho_{in}} \left[\rho_{in} E_{in}^{j-1/2} - \frac{1}{z_{n+1} - z_n} (\Delta E_{i,n+1}^{(z)} - \Delta E_{i,n}^{(z)}) \right.$$

$$\left. - \frac{2(r_{i+1} \Delta E_{i+1,n}^{(r)} - r_i \Delta E_{in}^{(r)})}{(r_{i+1} - r_i)(r_{i+1} + r_i)} \right.$$

$$\varepsilon_{in}^j = E_{in}^j - ((u_{in}^j)^2 + (v_{in}^j)^2)/2.$$

In the gas-dynamic stage of the solution the usual Courant limitation is imposed on the integration step τ.

4. THE RESULTS AND DISCUSSION

The mathematical technique presented in previous sections was applied to investigate the plasma behavior in air atmosphere with a pressure variation in the range 1–100 bar.

The radiation transfer in plasma (or in partially ionized gas) is closely connected with gas-dynamic and temperature fields, because the latter governs the optical thickness of the layer. In order to realize the multi-group approximation the determination of the group absorptivity coefficients $\kappa_k(T, \rho)$ in a wide range of temperature and pressure is required.

However, for the low-temperature air plasma, the description of these coefficients in terms of simple analytical

expressions is not available. The analysis of theoretical and experimental data [22] of the air absorptivity coefficients resulted in their tabular presentation for each group. The tabulation of beforehand-averaged absorptivity coefficients was performed for a given number of densities ρ_i, $1 < i < I$, $I = 8$, and temperatures T_j, $1 < j < J$, $J = 10$. The ranges of considered temperature and density values were equal: $T_j \in [1-20]$ eV and $\rho_i \in [10^{-4}-10^{-1}]$ g/cm^3. In calculations of the current values of T and ρ the absorptivity coefficients κ_{ij}^k are obtained by means of two-dimensional logarithmic interpolation. The frequency range taken into account lies in the region $h\nu = 0-40$ eV; it was divided into six groups. The assumed value of maximum temperature T_{max} was used to determine the upper boundary of frequency range and, consequently, the number of groups, by means of the relation $h\nu \approx 2.8\, T_{max}$. This relation is derived from the maximum value of Plank's function for spectral equilibrium density of radiation $U_{\nu, eq}$. It was assumed, that in the present case the plasma temperature does not exceed 10 eV.

Analogous tabular presentations are used for the equations of state $\varepsilon = \varepsilon(T, \rho)$, $P = P(T, \rho)$ [23], determined from the quantum-mechanical statistic models [24, 25].

The computational grid with the (34×35) total number of nodes is used for simulation. Along the r axis the grid nodes distribution is uniform. Along the z axis the grid nodes are condensed towards the target, according to the law of geometric progression with the factor $q = 1.1$.

The integration time-step τ_j was determined automatically in the course of solution with respect to the beforehand-fixed value of accuracy and the number of iterations.

Let us point out the following computational features of numerical algorithm. Almost 90% of the total run time is used for the averaging, for the solution of the multi-group diffusion and energy equation. The iteration process has not a high convergence rate, but it was found to be not sensitive to sharp variations of sought-for quantities, as, for example, $\kappa(T, \rho, \nu)$.

The chosen laser action parameters are typical for pulse laser processing of materials. The laser pulse (wavelength $\lambda = 1.06\ \mu$m) has a duration of $1\ \mu$s with a rectangular time-profile and Gaussian spatial distribution $G = G_0 \exp(-(r/R)^2)$ with the focal spot radius $R = 300\ \mu$m. The maximum intensity G_0 was varied in the range 10^7–10^8 W/cm^2.

When the ambient air pressure is $P_0 = 1$ bar, the initial plasma layer has the temperature $T_0 = 1.7$ eV and thickness $z_0 = 50\ \mu$m. At the first moments the incident laser radiation is almost entirely absorbed in the hot region. Due to the high density of the plasma layer, the plasma self-radiation is in fact locked and does not leave the hot region, that causes the sharp rise of the temperature and the pressure (up to $P_{max} \sim 3$ kbar). The high pressure difference induce an

intensive extension of the plasma layer in z-direction. The plasma density and pressure decrease, while the temperature still grows under the laser action up to the maximum value of $T_{max} \sim 8.5$ eV. At about $t \sim 10$ ns the shock wave arises at the boundary of the plasma with cold air, and at $t \sim 50$ ns the spreading of the hot region in a radial direction becomes noticeable. The plasma density decreases simultaneously with its temperature rise. This leads to the variation of the plasma optical properties and the rapid increase of the self-radiation role in the energy balance of the system.

The cold air at $T \sim 0.5$ eV is transparent for the visual spectrum radiation and for the near ultraviolet, but it strongly absorbs the radiation in the frequency range $hv = 10$–15 eV. Thus, if the temperature of the hot region is less than 3 eV, heating of the cold layers ahead due to self-radiation is insignificant. At the same time the magnitude of the radiation flux, propagating towards the target are governed to a large extent by the density of adjacent plasma layers and depends deeply on the regime of the gas-dynamic expansion.

The temperature isolines for the plasma pattern cross section at the moment $t = 65$ ns are presented in Fig. 1. The region involved in the shock wave is hatched and fringed with dotted lines. The velocity of the shock wave has already reached the maximum value $v_{max} \sim 3 \times 10^5$ cm/s and begins to decrease slowly. The temperature of the central region is slowly decreasing as well. The temperature isolines exhibit several regions, where dominant heating mechanisms vary. The central regions labeled 1 and 2 are heated by laser radiation. The regions 3 and 4 are heated by the compression forces' action, by the overall self-radiation flow W, and in part by the laser radiation. About 70% of the radiation emitted from the central regions is absorbed by the cold gas. The work of compression forces is not yet dominant in the energy exchange, as is illustrated by the semisphere-shaped temperature isolines. The total radiation flux towards the target is about 10% of G_0.

The geometry of the plasma pattern changes qualitatively at $t \sim 0.1$ μs. The isotherms at $t = 0.13$ μs are presented in Fig. 2. At this moment the direction of the gas-dynamic motion had been defined. The shock wave region is in close
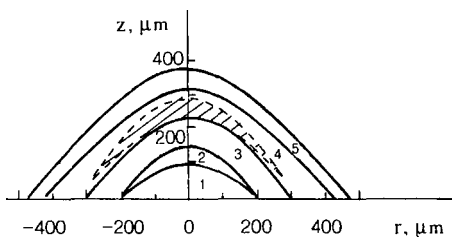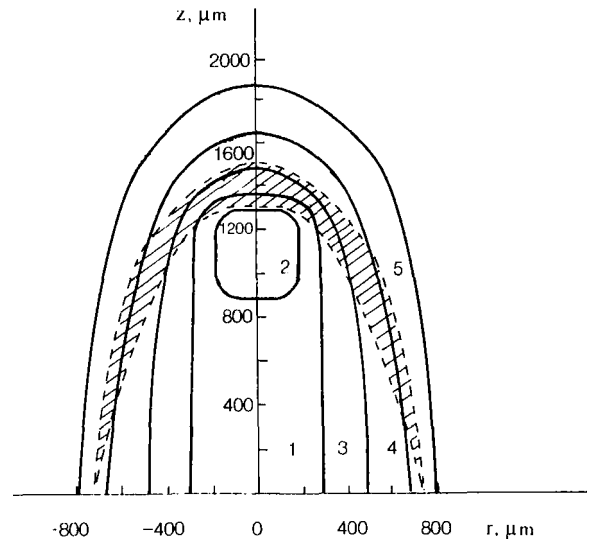
FIG. 2. Spatial temperature distribution in plasma pattern (initial pressure $P_0 = 1$ bar, $G_0 = 10^8$ W/cm^2) at time $t = 135$ ns. The temperature of the indicated areas: 1, 2.4 eV; 2, 3.0 eV; 3, 1.5 eV; 4, 0.4 eV; 5, 0.05 eV.

contact with the hot absorbing plasma layers. This forms the typical light-detonation complex, which influences the plasma pattern to obtain a cylindrical shape. Affected by gas-dynamic expansion the hot region breaks away from the surface and, due to the absorption of laser radiation, moves fast towards the source. Regions 1, 4, and 5 are heated mainly by radiation; region 3 is subjected to the combined action of compression forces, laser, and self-radiation. Nevertheless, spatial gas-dynamic expansion becomes dominant, which results in a substantial decrease of the temperature and of the pressure in the central regions. The total radiation flux W towards the target reaches 18% of G_0.

Later on, at $t > 0.5$ μs the plasma optical thickness decreases and the laser radiation again reaches the boundary $z = 0$, which is assumed to be the target surface.

It is necessary to note the high sensitivity of the laser–plasma interaction to the laser radiation intensity. The initially given plasma is not supplied enough by laser radiation and the light-detonation regime is not obtained if G_0 is reduced by one-half.

The process of the laser radiation interaction with plasma is strongly influenced by the ambient pressure of the gas medium (in the present case, air). Let us consider the situation when this pressure is two orders of magnitude higher (namely $P_0 = 100$ bar), the thickness of the original plasma layer is $z_0 = 15$ μm, all other parameters being equal. In this case at $t \sim 0.1$ μs the shock wave entirely breaks off the hot region; the temperature of the shock wave does not exceed 0.3 eV, and the maximum velocity $v_{max} \sim 2.4 \times 10^5$ cm/s, and it is entirely transparent to the laser radiation. The light-detonation mechanism is not obtained and the
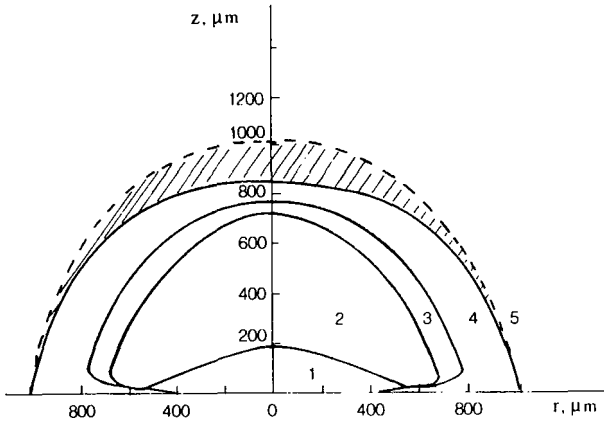
FIG. 1. Spatial temperature distribution in plasma pattern (initial pressure $P_0 = 1$ bar, $G_0 = 10^8$ W/cm^2) at time $t = 65$ ns. The temperature of the indicated areas: 1, 6.4 eV; 2, 7.0 eV; 3, 2.7 eV; 4, 0.9 eV; 5, 0.05 eV.

FIG. 3. Spatial temperature distribution in plasma (initial pressure $P_0 = 100$ bar, $G_0 = 10^8$ W/cm^2) at time $t = 0.5\,\mu$s. The temperature of the indicated areas: 1, 1.9 eV; 2, 4.5 eV; 3, 2.2 eV; 4, 0.1 eV; 5, 0.03 eV.

main propagation mechanism is the subsonic radiation wave [26].

The temperature isolines in the plasma region at $t = 0.5\,\mu$s are presented in Fig. 3. They indicate substantial plasma cloud expansion in the radial direction. The dynamics of the characteristic dimensions of the plasma cloud along the z-axis direction (Δz) and in the perpendicular direction r (Δr) is shown in Fig. 4. Figures 3 and 4 indicate that under an elevated pressure, the area and the contact time between the target surface and the chemically active plasma substance are significantly increased. The level of energy exchange due to the heat conduction and the radiation (with the spectral maximum about $h\nu = 10$ eV) is increased also. Note that the target surface is entirely screened from the laser radiation; that, on the one hand, prevents the former from destruction and, on the other hand, can increase the microhardness of the surface layers [27]. At the same time the results of the simulation show that the conditions of heat transfer and plasma action
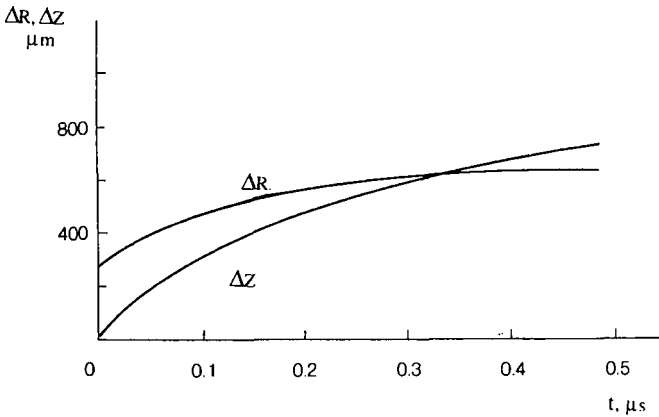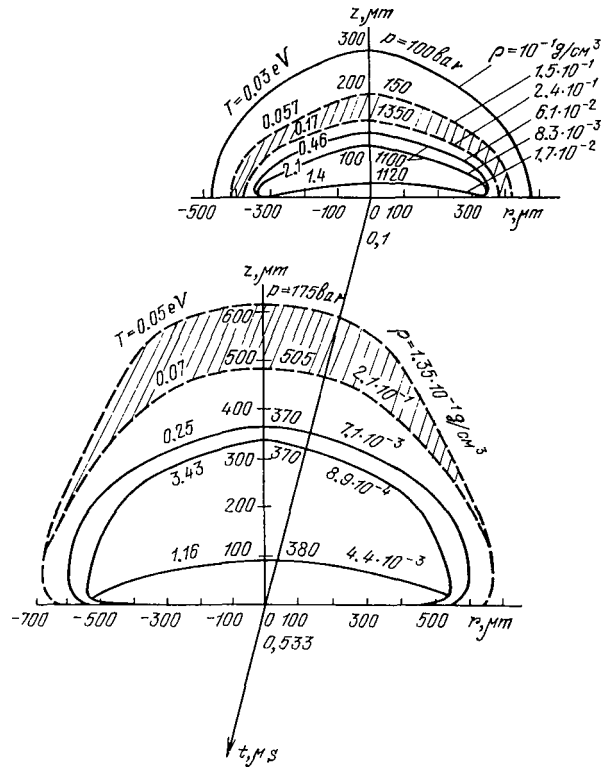

FIG. 5. Spatial distributions of: temperature T, pressure P, and density ρ in plasma (initial pressure $P_0 = 100$ bar, $G_0 = 5 \times 10^7$ W/cm^2).

are not optimal for two reasons: The hottest plasma layers are not in contact with the surface; the plasma cloud loses contact with the surface relatively fast.

The plasma pattern propagation can be delayed by a simple reduction of the intensity G_0. The spatial distributions of T, P, and ρ at two moments $t = 0.1\,\mu$s and $t = 0.5\,\mu$s after reducing G_0 by one-half (to $G_0 = 5 \times 10^7$ W/cm^2) are presented on Fig. 5. As in the previous case the main mechanism of the plasma propagation is the formation of
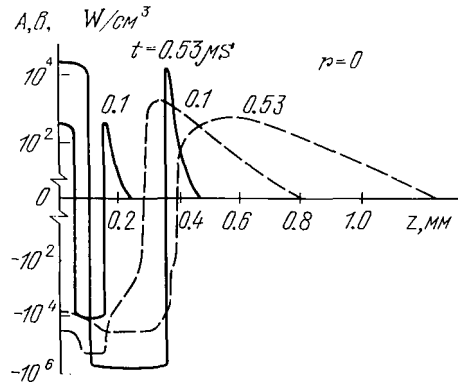

FIG. 4. Time dependence of the sizes of the plasma pattern along z and r axes (initial pressure $P_0 = 100$ bar, $G_0 = 10^8$ W/cm^2).

FIG. 6. Gas-dynamic (dashed curves) and radiative (solid line curves) components of plasma energy balance at $t_1 = 0.1\,\mu$s and $t_2 = 0.53\,\mu$s (initial pressure $P_0 = 100$ bar, $G_0 = 5 \times 10^7$ W/cm^2).

subsonic radiation waves. The laser radiation is entirely absorbed by the plasma layer. The maximum temperature of the hot region reaches the value of $T = 3.6$ eV, further growth being limited by the increase of emission. This is confirmed by comparison of the spatial distribution of two plasma energy components, namely radiative $B = (1/r)(\partial/\partial r)(rW_r) + \partial W_r/\partial z$ and gas-dynamic $A = P((1/r)(\partial/\partial r)(ru) + \partial v/\partial z)$ at two·time moments, as presented in Fig. 6. As a result of two-dimensional gas-dynamic plasma spreading, the area of the thermal action of the radiative flux appears to be several times larger than the focal spot. The maximum value of the acting flux does not exceed 5×10^5 W/cm^2, preventing the target from destruction. Nevertheless the surface does not still contact the hottest plasma layers; thus the degree of plasma-chemical action is reduced. From experimental observation [27–28] decrease of the pressure in a chamber to 30–50 bar could result in the destruction of the target's surface. As shown by computations, the reason for such a phenomenon at
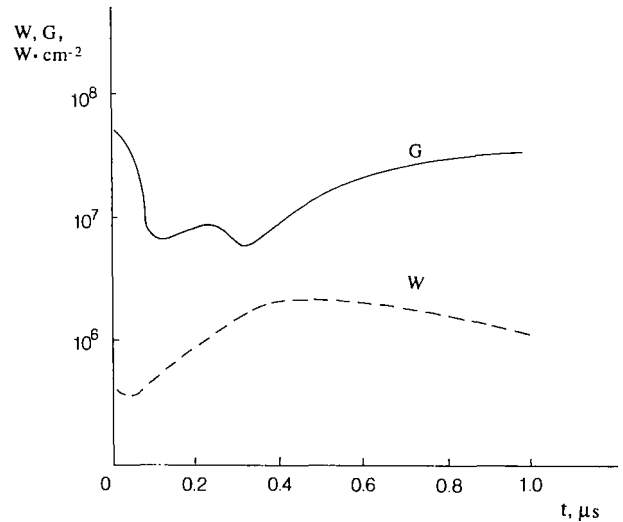

FIG. 7. Time dependence of laser (G) and radiation (W) energy fluxes reaching the surface of the target.
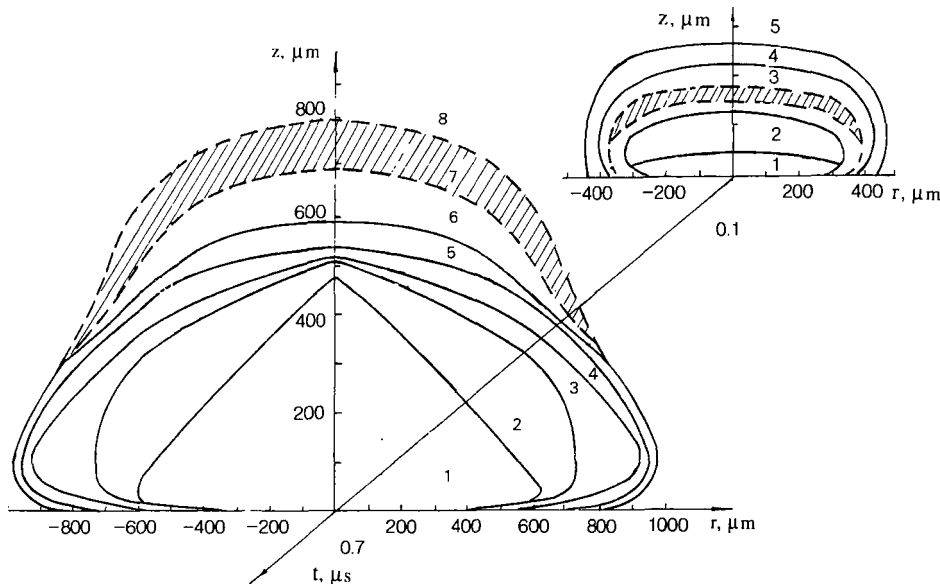

FIG. 8. Spatial distributions of: temperature T, pressure P, and density ρ in plasma pattern (initial pressure $P_0 = 30$ bar, $G_0 = 5 \times 10^7$ W/cm^2). The values of T, P, and ρ in the indicated areas are the following: at $t_1 = 0.1$ μs

  1. $T = 1.66$ eV, $P = 540$ bar, $\rho = 4.6 \times 10^{-3}$ g/cm^3;
  2. $T = 2.8$ eV, $P = 540$ bar, $\rho = 1.8 \times 10^{-3}$ g/cm^3;
  3. $T = 0.23$ eV, $P = 482$ bar, $\rho = 6.1 \times 10^{-2}$ g/cm^3;
  4. $T = 0.05$ eV, $P = 67$ bar, $\rho = 3.8 \times 10^{-2}$ g/cm^3;
  5. $T = 0.03$ eV, $P = 30$ bar, $\rho = 3 \times 10^{-2}$ g/cm^3;

at $t_2 = 0.7$ μs
  1. $T = 3.1$ eV, $P = 125$ bar, $\rho = 2 \times 10^{-4}$ g/cm^3;
  2. $T = 2.25$ eV, $P = 122$ bar, $\rho = 1.9 \times 10^{-4}$ g/cm^3;
  3. $T = 0.625$ eV, $P = 121$ bar, $\rho = 1.3 \times 10^{-3}$ g/cm^3;
  4. $T = 0.33$ eV, $P = 120$ bar, $\rho = 2.3 \times 10^{-3}$ g/cm^3;
  5. $T = 0.16$ eV, $P = 120$ bar, $\rho = 2.3 \times 10^{-3}$ g/cm^3;
  6. $T = 0.11$ eV, $P = 126$ bar, $\rho = 3.5 \times 10^{-3}$ g/cm^3;
  7. $T = 0.075$ eV, $P = 146$ bar, $\rho = 6 \times 10^{-2}$ g/cm^3;
  8. $T = 0.03$ eV, $P = 30$ bar, $\rho = 3 \times 10^{-2}$ g/cm^3;
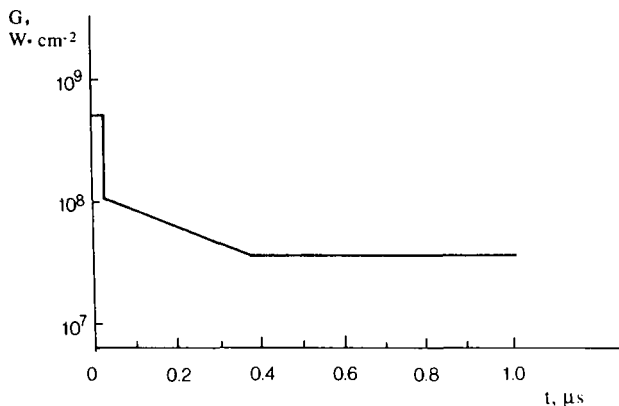
FIG. 9. The proposed laser pulse time-profile optimum for the maximum time of the contact between the hot plasma region and the target's surface.

$P = 30$ bar could be an intensive gas-dynamic spreading of the hot region. The initial stage of plasma development in the vicinity of the surface differs only slightly from the plasma behavior at $P = 100$ bar. The main part of the laser radiation is absorbed in the hot region; thus a complicated structure with different temperatures is built up.

The magnitude of the flux acting on the target lies in the range $(1-3) \times 10^6$ W/cm^2; the radius of interaction reaches the value of 600 μm. However, due to the lower density of the medium, the intensive expansion of the hot plasma produces such a decrease of the optical thickness that the laser radiation again reaches the surface at $t = 0.5$ μs. The time dependencies of the laser flux $G(t)$ and the total radiation flux $W(t)$ incident on the surface are presented in Fig. 7. They determine the surface temperature evolution. As consequences of the non-monotonic behavior of $G(t)$, the energy flux is substantially reduced at $t = 0.1-0.4$ μs due to the low-transparent plasma cloud. However, at the end of the pulse (< 1 μs) about 80% of the laser radiation reaches the surface due to the variation of the plasma optical thickness; that could result in target destruction. At the same time, when the pressure is $P_0 = 30$ bar, the surface contacts the hotest plasma regions during the entire pulse duration; see Fig. 8. The regime of the laser action can be optimized to eliminate the target destruction with simultaneous prolongation of the contact between the plasma and the target by setting the laser pulse time-profile proposed in Fig. 9 [29].

CONCLUSION

1. The proposed mathematical model describes the gas-dynamic stage of laser plasma evolution in air with the pressure varying in the range of $p = 1-100$ bar and the energy density flux of laser radiation varied in the range $G = 5 \times 10^7 - 5 \times 10^8$ W/cm^2 ($\lambda = 1.06$ μm).

2. The computational method (based on finite-differences) is used for the coupled solution of the equations of gas dynamics and radiation transfer in the multi-group diffusion approximation. The present approach proves its efficiency for simulation of the dynamics of radiative gas.

3. The computational experiment on laser–plasma interaction under controlled ambient pressure is a tool to determine different mechanisms of evolution and propagation of plasma patterns: from light-detonation at $P_0 = 1$ bar to subsonic radiation waves at $P_0 = 50-100$ bar. The plasma development at $P_0 = 10-30$ bar corresponds to the intermediate regime.

4. The total energy flux reaching the surface of the target (including the radiative component) is determined. The existence of a maximum of radiative energy flux versus the ambient gas pressure and energy density flux of laser irradiation is shown.

5. The optimal intensity–time profile of laser pulse to obtain: (a) the maximum radiative energy transfer into the target; (b) the maximum time of the contact between the hot plasma region and the target's surface, can be proposed.

REFERENCES

1. S. Marcus, J. E. Lowder, and D. L. Mooney, *J. Appl. Phys.* **47** 2966 (1976).

2. A. N. Pirri, R. G. Root, and R. S. Wu, *AIAA J.* **16**, No. 12, 1296 (1978).

3. G. Weyl, A. N. Pirri, and R. S. Wu, *AIAA J.* **19**, No. 4 460 (1981).

4. Y. P. Raiser, *Sov. Phys. JETP* **48**, No. 5, 1508 (1965).

5. Y. P. Raiser, *Sov. Phys. JETP* **31**, No. 6, 653 (1970).

6. R. V. Amburcumjan, N. G. Basov, V. A. Bojko, *et al. Sov. Phys. JETP* **82**, No. 3, 1583 (1970).

7. U. P. Raiser, *Uspekhi Phys. Nauk.* **87**, No. 1, 29 (1964).

8. G. A. Askarjan, M. S. Rabinovich, M. M. Savchenko, and A. D. Smirnov, *Sov. Phys. Lett. JETP Lett.* **1**, No. 6, 18 (1965).

9. J. P. Jackson and P. E. Welsen, *AIAA J.* **12**, No. 11, 1498 (1974).

10. G. Grimm, *Plasma Spectroscopy* (Atomizdat, Moscow, 1969).

11. J. B. Zeldovich and Y. P. Rajzer, *Physics of Shock Waves and High-Temperature Gas Dynamic Phenomena* (Nauka, Moscow, 1966).

12. T. Holstein, *Phys. Rev.* **72**, No. 12, 1212 (1947).

13. L. M. Biberman, *Sov. Phys. JETP* **17**, 416 (1947).

14. V. I. Derzhiev, A. G. Zhidkov, and S. I. Jakovenko, *Radiation of Ions in Nonequilibrium Dense Plasma* (Energoatomizdat, Moscow, 1986), 159.

15. V. I. Mazhukin, A. A. Uglov, and B. N. Chetveruskin, *Dokl. Akad. Nauk SSSR* **256**, No. 5, 1100 (1981).

16. M. I. Volchinskaja, V. I. Mazhukin, B. N. Chetveruskin, and N. G. Churbanova, *JVM i MP*, **23**, No. 5, 1177 (1983).

17. M. I. Volchinskaja and B. N. Chetveruskin, *JVM i MP*, **19**, No. 5, 1262 (1979).

18. V. Ja Goldin and B. N. Chetveruskin, *JVM i MP*, **12**, No. 4, 990 (1972).

19. M. I. Volchinkaja and B. N. Chetveruskhin, *JVM i MP*, **17**, No. 2, 248 (1977).

20. R. A. Jentry, R. E. Martin, and B. I. Daly, *J. Comput. Phys.* **6**, 87 (1966).

21. B. P. Gerasimov, S. A. Semushin, *Differen. Uravneniya* 17, No. 7, 1214 (1981).

22. V. A. Kamenshikov, J. A. Plastinin, V. M. Nikolaev, and L. A. Novickij, *Radiative Properties of Gases at High Temperatures* (Mashinostroenije, Moscos, 1971).

23. N. N. Kalitkin, L. V. Kuzmina, and V. S. Rogov, Preprint IMP AN SSSR, 1972.

24. A. V. Bushman and V. E. Fortov, *Uspekhi Phys. Nauk* 140, No. 2, 177 (1983).

25. L. V. Altshuler, A. V. Bushman, M. V. Jernokletov, V. N. Zubarev, and A. A. Leontiev, *Sov. Phys. JETP* 78, No. 2, 741 (1980).

26. E. A. Kozik, T. V. Loseve, I. V. Nemchinov, and V. V. Novikova, *Kvantovaya Electron.* 5, No. 10, 2138 (1978).

27. I. Smurov, A. Smirnov, A. Ferriere, and G. Flamant, on *Proceedings, 10th International Symposium on Plasma Chemistry, Bochum, Germany, 1991,* 1.3–7, pp. 1–6.

28. I. Smurov, A. Uglov, P. Matteazzi, F. Miani, and N. Tosto, in *Proceedings, 10th International Symposium on Plasma Chemistry, Bochum, Germany, 1991,* 1.4–28, pp. 1–6.

29. V. I. Mazhukin, N. N. Rykalin, A. A. Uglov, and B. N. Chetveruskhin, "Technique of Gas Nitrading of Metals Parts," Patent No. 1034428, 1982, pp. 1–5.